Nano Res. 2012, 5(12): 903–916
DOI 10.1007/s12274-012-0274-6
Research Article

ISSN 1998-0124
CN 11-5974/O4

From Zero to Two Dimensions: Supramolecular Nanostructures Formed from Perylene-3,4,9,10-tetracarboxylic Diimide (PTCDI) and Ni on the Au(111) Surface Through the Interplay Between Hydrogen-Bonding and Electrostatic Metal–Organic Interactions

Miao Yu[1,4], Wei Xu[1], Nataliya Kalashnyk[1], Youness Benjalal[2,3], Samuthira Nagarajan[2], Federico Masini[1], Erik Lægsgaard[1], Mohamed Hliwa[2,3], Xavier Bouju[2], André Gourdon[2], Christian Joachim[2], Flemming Besenbacher[1] (✉), and Trolle R. Linderoth[1] (✉)

[1] Interdisciplinary Nanoscience Center (iNANO) and Department of Physics and Astronomy, Aarhus University, Aarhus 8000, Denmark
[2] Nanosciences group, CEMES-CNRS, Toulouse 31055, France
[3] Faculté des Sciences Ben M'Sik, Université Hassan II-Mohammédia, Casablanca BP 7955, Morocco
[4] School of Chemical Engineering and Technology, Harbin Institute of Technology, Harbin 150001, China

Received: 3 August 2012 / Revised: 11 October 2012 / Accepted: 25 October 2012

ABSTRACT

Supramolecular self-assembly of the organic semiconductor perylene-3,4,9,10-tetracarboxylic diimide (PTCDI) together with Ni atoms on the inert Au(111) surface has been investigated using high-resolution scanning tunneling microscopy under ultrahigh vacuum conditions. We demonstrate that it is possible by tuning the co-adsorption conditions to synthesize three distinct self-assembled Ni–PTCDI nanostructures from zero-dimensional (0-D) nanodots over one-dimensional (1-D) chains to a two-dimensional (2-D) porous network. The subtle interplay among non-covalent interactions responsible for the formation of the observed structures has been revealed from force-field structural modeling and calculations of partial charges, bond orders and binding energies in the structures. A unifying motif for the 1-D chains and the 2-D network is found to be double N–H···O hydrogen bonds between PTCDI molecules, similar to the situation found in surface structures formed from pure PTCDI. Most interestingly, we find that the role of the Ni atoms in forming the observed structures is not to participate in metal–organic coordination bonding. Rather, the Ni adatoms acquire a negative partial charge through interaction with the substrate and the Ni–PTCDI interaction is entirely electrostatic.

KEYWORDS

perylene-3,4,9,10-tetracarboxylic diimide (PTCDI), molecular self-assembly, hydrogen bonding, electrostatic interaction, scanning tunneling microscopy

1. Introduction

Controlled self-assembly of complex supramolecular surface architectures has considerable potential for application in many fields within the quickly-emerging area of nanoscience and technology, including heterogeneous catalysis, gas storage, chemical sensing, surface-templating, molecular recognition,

Address correspondence to Trolle R. Linderoth, trolle@inano.au.dk; Flemming Besenbacher, fbe@inano.au.dk

opto-electronics, and host–guest chemistry [1–4]. By adopting different building blocks, a wide range of supramolecular structures have been investigated under ultrahigh vacuum (UHV) conditions and characterized using scanning tunneling microscopy (STM). Versatile strategies have been employed to fabricate well-ordered and highly hierarchical molecular nanostructures on suitable substrates using non-covalent interaction, allowing for massively parallel bottom-up synthesis [5–39]. In particular, stimulated by the ubiquity in biological systems, hydrogen bonding (H-bonding) and van der Waals (vdW) interactions have been exploited widely [5–11]. Another important approach for supramolecular engineering is to grow surface-confined metalloorganic structures by co-deposition of organic molecules and metal adatoms [12–39]. This approach has been explored systematically over the last decade, most notably resulting in hierarchically assembled structures [12–39] and highly ordered metal–organic surface networks with pore sizes and symmetries that are tunable through appropriate choice of substrate, organic ligands and transition metal centers [13, 15–17, 28, 35]. Such structures have in many cases been rationalized from qualitative two-dimensional adsorption models [13, 16, 17, 35–37], while selected studies addressing the detailed nature of the metal–organic interaction have been performed based on photo–electron [15] or scanning tunneling spectroscopy [32]. Complementary theoretical modeling has often focused on free-standing metal–organic structures [12, 38] to reduce the computational load but in certain cases the adsorbate–substrate interaction has been taken into account by modeling the surface as clusters [28] or slabs [21] of atoms. In general, these studies have confirmed the picture of coordination bonding between metal centers and ligands, e.g., for Fe–carboxylate [15], Cu–1,3,8,10-tetraazaperopyrene (TAPP) [30], Cu–thiolate [31], Co-dicyanoazobenzene [32] and Cu–9,10-anthracenedicarbonitrile (DCA) [39]. The charge state of the adsorbed coordinating metal centers are generally found to be positive [15, 30] or close to neutral [32] while one case of a negatively charged center has been observed for Cu/Cu(111) coordinating to anthracenedicarbonitrile molecules [39].

In this study, we investigate metal–organic self-assembly of perylene-3,4,9,10-tetracarboxylic diimide (PTCDI, see Fig. 1(a)) and Ni on the Au(111) surface using high-resolution STM under ultrahigh vacuum (UHV) conditions. The molecule PTCDI and its derivatives are technologically relevant owing to their interesting opto-electronic properties [40, 41], and their adsorption properties have been investigated on a wide range of substrates [42–48] as fundamental model systems for understanding the interaction of large aromatic molecules with inorganic surfaces. Studies of binary or ternary molecular assemblies formed from PTCDI and other molecules through complementary H-bonding have also been performed [7, 26, 49–51]. Co-adsorption of PTCDI with metal atoms (Ni) was studied recently and a number of

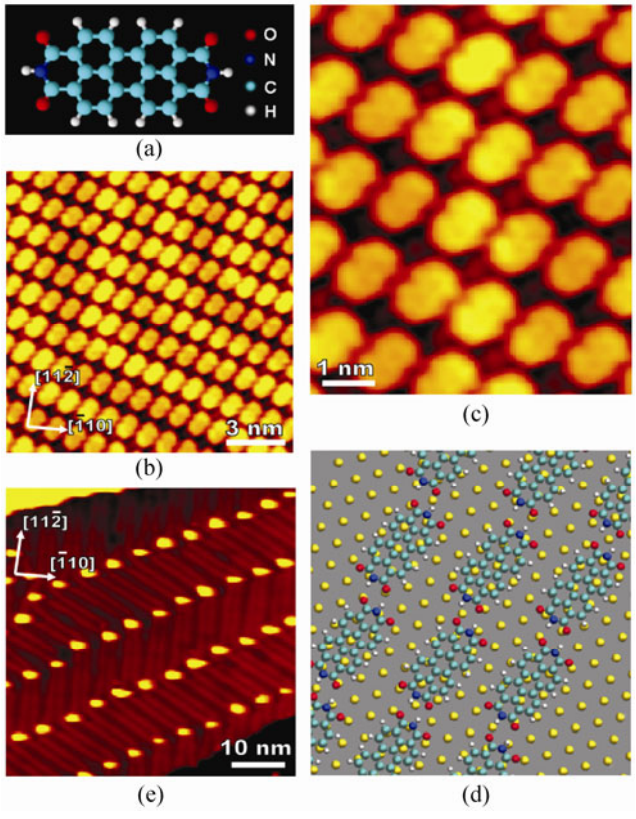

Figure 1 (a) Chemical structure of perylene-3,4,9,10-tetracarboxylic diimide (PTCDI). (b) STM image of an extended PTCDI island formed on a Au(111) terrace (I_t = 0.41 nA, V_t = 1.25 V). (c) High-resolution STM image of the PTCDI structure (I_t = 0.41 nA, V_t = 1.25 V). (d) Optimized model of close-packed PTCDI arrangement on Au(111) after full relaxation with the MM4 force-field method, revealing that PTCDI are aligned into rows in a head-to-tail style by intermolecular double hydrogen bonding (Au atoms are represented by yellow balls). (e) STM image of monolayer-height Ni clusters at a coverage of ~0.05 ML nucleated at the elbow sites of the Au(111) herringbone reconstruction (I_t = 0.38 nA, V_t = 1.25 V)

structures attributed to metal–organic coordination were observed at limited resolution by STM [36].

Our study shows that it is possible by delicately tuning the co-adsorption conditions to synthesize three distinct self-assembled Ni–PTCDI nanostructures from zero-dimensional (0-D) nanodots to one-dimensional (1-D) chains to a two-dimensional (2-D) porous network. In general, the ability to generate a diverse range of nanostructures of different dimensionality from the same elementary building blocks is important since it may help to simplify synthesis of nanostructures for practical applications. To achieve a full picture of the interactions driving the formation of the observed Ni–PTCDI structures, we have performed molecular mechanics and quantum chemical calculations, as well as STM image calculations. A unifying motif for the 1-D Ni–PTCDI chains and the 2-D Ni–PTCDI network is found to be double N–H···O hydrogen bonds between PTCDI molecules arranged in staggered rows, similar to the situation found in surface structures formed from pure PTCDI. Most interestingly, we find that while Ni co-deposition with PTCDI is essential to form the observed structures, the role of the Ni adatoms is not to participate in metal–organic coordination bonding as cationic centers. Rather, the Ni adatoms acquire a negative partial charge through interaction with the substrate and the Ni–PTCDI interaction is entirely electrostatic.

2. Experimental

STM measurements were performed using a variable-temperature Aarhus STM [52], mounted in a UHV chamber with a typical base pressure of 1×10^{-10} Torr. The Au(111) single-crystal sample was cleaned by repeated cycles of 1.5 keV Ar^+ ion bombardment and annealing to 850 K for 15 min. PTCDI molecules were deposited from a glass crucible wound with a Ta wire for resistive heating and with a thermocouple pair fused into the glass for temperature monitoring. The evaporator was held at 600 K during sublimation. Ni was evaporated from a 99.99% pure resistively heated Ni wire. Molecular and atomic coverages were estimated from STM images as fractions of a saturated first layer (ML) for the respective species on the Au(111) surface. All STM images presented here were collected in the constant current mode and acquired at a sample temperature of approximately 110 K using an electrochemically etched polycrystalline W tip.

For the computational part we adopted the following strategy. First, we calculated the conformation of a single molecule adsorbed above a single layer Au(111) surface and surrounded by four nickel atoms by *ab initio* calculations at the SCF-MP2(TZVP) level with the GAMESS code [53]. We established with this simple system that neither covalent nor coordination bonding is responsible for the adsorption due to a too large interatomic distance between the Ni atoms and the molecule. This means that *ab initio* calculations would become prohibitively expensive as we have to deal with large supramolecular structures adsorbed on a metallic surface. For the supramolecular optimization we have therefore used force-field calculations such as MM4 [54, 55] with a substrate containing four gold layers (we have checked that a larger slab does not provide noticeable differences). At this stage, STM images of the obtained geometries have been systematically calculated and compared to experimental images: Molecular structures are validated once the agreement between calculated and experimental images is found qualitatively correct. If needed for the detailed understanding, *ab initio* calculations (without geometrical optimization) were performed starting from the force-field calculated conformations to determine for instance the partial charges on the atomic sites and the bond orders between the molecule and the substrate, or the H-bonding interaction in comparison with MM4 calculations. Molecular adsorption energies were calculated with the MOPAC-2009 code [56] at the PM6 level adapted for transition metal and H-bonding and the MM4 force field [54] without and with nickel adatoms on the surface. As results obtained with the two methods compared well, the MM4 method was used for intensive calculations. Additionally, the intermolecular contribution to the total interaction energy is calculated with the help of the MM4 force field that includes directional H-bonding. Mulliken partial charges and bond orders were evaluated using SCF-PM6 approximation. Calculation of STM images was performed using the ESQC-STM code [57, 58]. This method has already

demonstrated its efficiency and reliability to deal with STM image calculations not only with small systems [59] but also with large adsorbed molecules [60].

3. Results and discussion

We first describe results for PTCDI alone on the Au(111) surface, an adsorption system which has been investigated before in several instances [7, 36, 45, 48, 61]. In the present case, the molecules were deposited onto a Au(111) surface kept at room temperature, followed by a post-annealing at 400 K for 10 min and cooling to 110 K. This resulted in well-ordered, mono-molecular high islands as depicted by the STM images in Figs. 1(b) and 1(c). Each elongated feature within this structure is attributed to an individual PTCDI molecule adsorbed with its plane parallel to the surface. The PTCDI molecules adopt a head-to-tail arrangement into rows which again pack sideways to form the observed extended domains. The spacing between centers of neighbouring molecules is 1.4 ± 0.1 nm along the row direction and 1.1 ± 0.1 nm between two neighbouring rows. The long axis of the molecules is rotated slightly (~12°) with respect to the direction of the molecular rows. The herringbone reconstruction of the Au(111) substrate is not significantly perturbed by the adsorption of the PTCDI molecules, as judged from a characteristic modulation of the molecular corrugation clearly observed in large scale images, e.g., in Fig. 1(b).

Calculations were performed to establish the intermolecular and molecule–surface interactions responsible for the formation of the described PTCDI structure, and also to act as a starting point for further modeling of Ni–PTCDI structures. The optimum adsorption site for a single PTCDI molecule is found from MM4 force-field calculations [54, 55] to be an atop site on the Au(111) surface, i.e., with its central aromatic ring located above a gold atom. In this position, the minimal adsorption energy is –2.56 eV and the molecule–substrate distance is 3.80 Å (the adsorption height is defined as the distance between the outermost lattice plane of the substrate and the plane formed by the central benzene ring). These results are consistent with previous calculations for perylenetetracarboxylic dianhydride (PTCDA), a close analog of PTCDI [62]. A model for the extended PTCDI structure on the Au(111) surface was obtained from MM4 calculations and is shown in Fig. 1(d): Starting with a molecular arrangement involving molecules in the optimum atop positions, one finds after full relaxation an alignment into rows, allowing for double N–H···O H-bonding interaction between the imide and carboxyl groups of neighbouring PTCDI molecules along the rows. The calculated structure has a unit cell size of 1.15 ± 0.02 nm (inter-row) by 1.40 ± 0.01 nm (intra-row), and the angle between the molecular axis and the row axis is 12.2° ± 0.5°, and approximately 12° between the row axis and the $[\bar{1}10]$ direction of the surface, all consistent with the experimental observations. In order to validate the MM4 H-bonding parameterization, we have checked the double N–H···O H-bonding in the head-to-tail configuration of two PTCDI molecules, as shown in Fig. 1(d), which can be accurately described from *ab initio* calculations at the SCF-MP2 (TZVP) level with the GAMESS code [53]. The bond length between two molecules, that is to say the N–H···O distance, is 2.64 Å in agreement with the full structural model. The stabilization energy is –0.41 eV for two molecules joined by double N–H···O hydrogen bonds, consistent with recent density functional theory (DFT) calculations (which is at a comparable accuracy level as the MP2 description) for a gas phase dimer of cyanuric acid [63] and of PTCDI [45], respectively. Notice that similar results were already obtained with the MM4 force field following parameterization in Ref. [64]. As it is difficult to take into account vdW interactions by *ab initio* methods, we have also evaluated the inter-row interaction from force-field calculations with MM4 [54]. This shows that the interaction energy at a row-to-row distance of 11.5 Å is dominated by vdW forces and is –0.120 eV per pair of molecules. Comparing to previous studies of PTCDI on Au(111) [7, 45, 48], there is generally an agreement on the arrangement with H-bonded rows formed from molecules slightly rotated compared to the row direction. However, significant variations have been observed in the inter-row arrangements, in particular opposite sense of rotation for molecules in adjacent rows and/or larger lateral shift of adjacent rows along the row direction, leading to brick-wall structures. The structures most resembling the one reported here were

found on narrow terraces of vicinal Au(11,11,12) [7]. Together, these experimental observations support a comparatively weak inter-row coupling, such that subtle differences in the experimental preparation conditions (substrate temperature, deposition rate, local coverage) can lead to the observed variation in inter-row stacking, while the intra-row interactions are stronger and create a robust intra-row stacking motif, in agreement with the interaction energies presented above.

Deposition of Ni atoms alone leads to isolated Ni clusters, as shown in the STM image of Fig. 1(e). The Ni atoms were deposited at a coverage of ~0.05 ML (ML = monolayer) on an Au(111) substrate kept at room temperature, followed directly by cooling to 110 K without post-deposition annealing. The Ni clusters have an average size of 3.0 nm and are found exclusively at the bulged elbow sites of the Au(111) herringbone reconstruction. Selective nucleation of transition metal islands at the elbow sites of the Au(111) herringbone reconstruction is well known, and such arrays of dispersed clusters have been used before as nanostructuring templates for supramolecular fabrication and a source of metal atoms for metal–organic molecular architectures [13, 15–17, 35].

Next, we discuss the situation for low-coverage co-deposition of PTCDI (~0.03 ML) and Ni (~0.01 ML) on the Au(111) surface. In the experiments, the two species were deposited simultaneously onto an Au(111) substrate kept at room temperature followed directly by cooling to 110 K without post-deposition annealing. As shown in the STM image of Fig. 2(a), this leads to quasi-0-D triangular nanoclusters on the surface, predominantly aligned at or nearby the bulged elbow sites of the Au(111) substrate. The clusters disappear if a post-deposition annealing is applied, indicating that they are kinetically trapped. Small islands of PTCDI molecules (with/without Ni) as well as additional Ni clusters can also be observed, in particular if the ratio of the two components is varied and the coverage is slightly increased.

The high-resolution STM image in Fig. 2(b) shows that each cluster consists of three ellipsoidal features arranged to form the sides of a triangle surrounding a central protrusion. Since these clusters are distinctly different from those formed from Ni and such clusters are never observed when PTCDI is deposited alone, we conclude that they involve both Ni and PTCDI species. To obtain quantitative information about the PTCDI–Ni cluster configurations, MM4 molecular mechanics calculations were performed. Figure 2(c) shows an optimized cluster motif on the Au(111) surface involving three PTCDI molecules surrounding a central Ni atom. A calculated STM image of this configuration is shown in Fig. 2(d), and is in qualitative and quantitative agreement with the STM data for the clusters as shown in Fig. 2(b). At this point, one may infer that force-field calculations with the present parameterization give realistic molecular arrangements.

In the calculated configuration, the Ni atom is kept fixed in a three-fold hollow site of the Au(111) substrate at an adsorption height of 1.8 Å [65, 66], corresponding to a Ni–Au center to center distance of 2.5 Å. (Given the interatomic Ni–Au distance in a bulk Ni–Au alloy

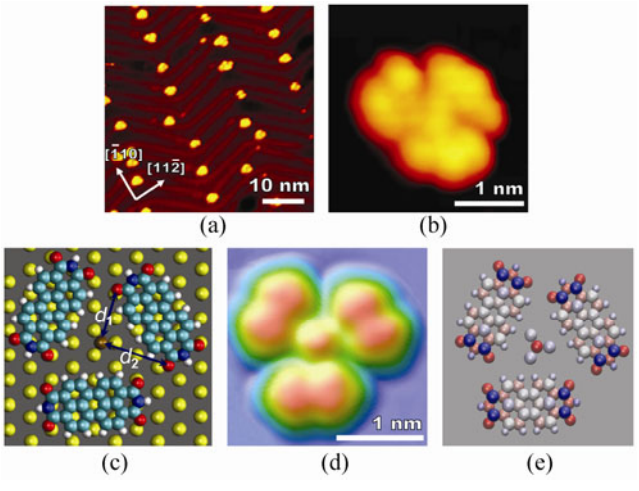

Figure 2 (a) STM image of PTCDI/Ni clusters decorating the bulged elbows of the Au(111) herringbone reconstruction (I_t = 0.83 nA, V_t = 1.49 V). (b) High-resolution STM image of the triangular cluster, consisting of three ellipse-like features corresponding to PTCDI molecules and a circular central core attributed to a single Ni atom (I_t = 0.55 nA, V_t = 1.05 V). (c) Optimized model of this nanocluster on Au(111) after full relaxation with the MM4 force-field, PTCDI molecules surround a single Ni atom (brown ball). (d) Calculated STM image of a relaxed PTCDI/Ni cluster obtained by the EHMO-ESQC method and at the same imaging parameters as used in panel b. (e) Partial charges distribution for the cluster shown in panel c. Only three gold atoms below the central Ni atom are shown while the other surface atoms with a partial charge close to zero are omitted for clarity. The color scale from dark blue to red corresponds to +0.63|*e*| to –0.61|*e*| and gray color indicates neutral atoms

of 2.6–2.7 Å [67], we have considered a reasonable and realistic relaxation of the Ni atom on the surface, leading to a Ni–Au distance of 2.5 Å.) The Ni adatom is surrounded by three PTCDI molecules calculated to be somewhat further away from the surface at a height of 3.80 Å. In this configuration, each PTCDI molecule has the two oxygen atoms on one side of the molecular axis pointing towards the central Ni atom. However, the Ni···O distances, which fall in two classes as seen in Fig. 2(c) d_1 = 6.75 ± 0.08 Å and d_2 = 8.56 ± 0.03 Å, are much too large to allow for significant electron cloud overlapping between the Ni and O atoms. To assess a possible contribution from electrostatic interactions, accurate PM6 calculations were performed to obtain the Mulliken partial charges on every atomic site of the MM4 optimized structure. The Ni atom in the hollow surface site is at the apex of a tetrahedral $NiAu_3$ cluster involving the three underlying Au surface atoms. The central Ni atom exhibits a net negative charge of –0.61|*e*| that is almost compensated for by the positive charges of the three underlying Au atoms which is +0.16|*e*| per atom on average while the other surface atoms are found to have a very low negative charge (Fig. 2(e)). (See below for discussion of the negative charge state for the Ni atoms). The 1($NiAu_3$)···3(PTCDI) electrostatic interaction between the charges on the atoms of the three molecules and the atoms of the whole surface including the $NiAu_3$ cluster is attractive with an interaction energy of –0.8 eV, corresponding to –270 meV for a Ni···PTCDI pair. For this reason, and because of the lack of coordination interaction, the Ni···O interaction is exclusively electrostatic. This is consistent with the crystal field interaction model [68, 69]. Finally, the intermolecular interaction within the cluster has to be considered. The optimized model exhibits three C–H···O hydrogen bonds with a bond length of 3.3 Å and an attractive energy of –0.1 eV each. Additionally, vdW interaction provides –0.5 eV for the 3 PTCDI molecular cluster (obtained by summing up all the atom–atom interactions in the system with MM4 parameters). Thus, the total intermolecular contribution to the cohesion energy of the cluster is approximately –0.8 eV. In contrast to the situation of pure PTCDI structures, N–H···O hydrogen bonds do not lead to the cohesion in the clusters since these moieties are separated too far and are in an unfavourable geometry; the average N–O separation is 5.37 ± 0.10 Å with an angle of 124 ± 1°. In summary, the analysis of binding energy shows that the internal cluster structure is governed by vdW intermolecular interaction with a minor contribution from C–H···O H-bonding while the stability of the cluster on the surface owes to electrostatic interactions. We speculate that the role of the Ni atoms is most likely to provide nucleation sites, i.e., diffusing Ni atoms adsorbed at the bulged elbows sites on the herringbone reconstructed Au(111) terraces allow trapping of molecules and growth of the organic nanodots.

Co-deposition at intermediate coverage of PTCDI (~0.1–0.3 ML) and Ni atoms (~0.03–0.05 ML) either simultaneously or sequentially (Ni followed by PTCDI), leads to 1-D chains on the Au(111) surface as shown in the STM image of Fig. 3(a). The deposition was carried out on a substrate kept at room temperature and the 1-D chains were observed after post-deposition annealing at 400 K for 10 min followed by cooling to 110 K where the STM images were acquired. The chains extend over ~50 nm and are aligned essentially along the $<11\bar{2}>$ type directions, either parallel to the ridges or across the elbows of the herringbone reconstruction, without disturbing the underlying substrate. The typical separation of neighbouring chains is ~3–4 nm. These isolated chains are distinctly different from the compact and ordered 2-D islands formed from PTCDI alone.

A high-resolution STM image of a 1-D chain is displayed in Fig. 3(b), showing large elongated protrusions aligned with their long axis approximately along the chain direction and decorated by smaller protrusions to the sides of the chain at the positions where the larger protrusions join. We attribute the large protrusions to PTCDI molecules and the smaller protrusions to individual Ni adatoms. The PTCDI molecules in the chains have the same periodicity of 1.4 ± 0.1 nm as observed in the pure PTCDI structure. A line connecting two Ni protrusions on opposite sides of the chain cuts the main axis of the chain at an angle slightly off orthogonal (~103°) and four Ni protrusions define a parallelogram of (1.0 ± 0.1) nm × (1.4 ± 0.1) nm dimensions, surrounding a PTCDI molecule.

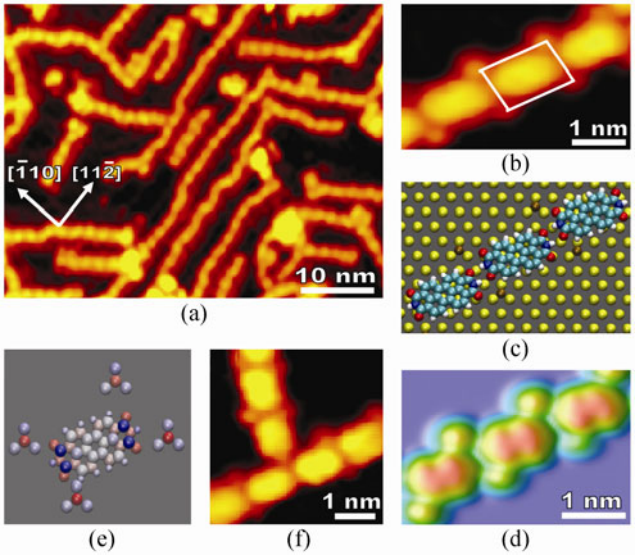

Figure 3 (a) STM image of PTCDI/Ni chains extended over 50 nm, along the ridges or across the elbows of Au(111) herringbone reconstruction (I_t = 0.70 nA, V_t = 1.24 V). (b) High-resolution image of the filament, consisting of ellipse-like features attributed to PTCDI molecules with Ni atoms located on both sides at the junction between neighbouring PTCDI molecules (I_t = 0.53 nA, V_t = 1.20 V). (c) Optimized model for the Ni–PTCDI chain calculated by the MM4 force field after full relaxation: The Ni atoms occupy hollow sites at a fixed distance of the gold surface (1.8 Å) and the center of PTCDI is at atop sites. (d) Calculated STM image of the shown Ni–PTCDI chain consistent with the experimental results. (e) Partial charges distribution of the central molecule in panel c surrounded by four Ni adatoms. Only twelve gold atoms are shown and the other surface atoms with a partial charge close to zero are not shown for clarity. The colors scale from dark blue to red corresponding to +0.62|*e*| to –0.65|*e*|, respectively, and gray color stands for neutral atoms. (f) STM image of "T-shape" Ni–PTCDI junction (I_t = 0.44 nA, V_t = 0.71 V)

The Ni–PTCDI chains are observed to co-exist with PTCDI islands and Ni clusters on the surface. The relative yield of these phases depends on the coverage and the annealing process. Higher coverage and less annealing treatment (shorter duration and lower temperature of annealing) results in a higher degree of phase separation. The chains form after annealing both for sequential and simultaneous deposition, suggesting that the pure PTCDI and Ni structures partially decompose during annealing and the chains grow from the species liberated.

Theoretical modeling of the chain structure started from identifying a possible Ni mesh on the Au(111) surface based on the periodicity and orientation of the Ni mesh obtained experimentally (the reconstruction of the Au(111) substrate was not taken into account). Ni atoms are found to be at hollow sites of the Au(111) substrate forming a mesh with dimensions of 1.04 nm × 1.50 nm and an included angle of 104°, consistent with the experimental data. Then three PTCDI molecules were placed inside the mesh formed from eight Ni adatoms and the PTCDI positions were relaxed with the MM4 method, including molecule–molecule, molecule–Au substrate and molecule–Ni interactions, as one can see above that the parameterization is precise enough for this system. Figure 3(c) shows the optimum geometry obtained after full relaxation of the molecular system. The PTCDI molecules are aligned with their main axis 12° away from the axis of the molecular row and the molecular centres are adsorbed near atop sites of the Au(111) substrate. A calculated STM image based on this optimized model is presented in Fig. 3(d), showing good agreement with the experimental image of Fig. 3(b). The interaction between two adjacent PTCDI molecules in the chain is provided by intermolecular double N–H···O H-bonding, identical to the case of pure PTCDI rows, as shown by MM4 calculations. Based on both STM data and our calculation results, the distances between the oxygen atoms of the PTCDI molecules and the Ni adatoms appear too large to invoke Ni–O electron transfer: If only considering the Ni···O distance in a plane parallel to the surface, as one might do from STM images and qualitative 2D adsorption models, the Ni···O distance could be 3.3 Å. However, considering the length of the Ni–O vector in 3D, the different adsorption heights of PTCDI and Ni make the calculated shortest Ni–O distance 3.9 Å, which rules out the possibility of coordination bonding.

Similar to the case of the cluster, the distribution of Mulliken partial charges (see Fig. 3(e)), as well as different bond orders, were evaluated from PM6 calculations [70] for one PTCDI molecule surrounded by four Ni adatoms in the geometry of Fig. 3(c). The average net charges are –0.58|*e*| for the oxygen atoms closest to Ni and –0.62|*e*| to –0.65|*e*| for the Ni atoms themselves. The net charges on the carbon and the hydrogen atoms depend on their respective positions in the molecular system. The net charge of the Au surface atoms is nearly equal to zero, except for the

three Au atoms surrounding every Ni atom which are found to carry a positive charge of +0.20|*e*| each. Notice that the overall Au charges compensate for the negative charge on Ni preserving the $NiAu_3$ cluster neutrality, and the negative charge on the O atoms is similarly compensated for by positive charge on the molecular system, in particular the carbon atoms next to the oxygen atoms (Fig. 3(e)). The total electrostatic interaction (i.e., without the vdW contribution) between a single molecule, four Ni adatoms of the mesh and the gold surface [4($NiAu_3$)···1(PTCDI) system] leads to an overall attractive energy of –30 meV. This binding energy is considerably lower than for the previously described 1($NiAu_3$)···3(PTCDI) case in the 0-D clusters, owing to reduced distances between O and Ni atoms. As this distance changes from 6.75 Å (clusters) to 3.93 Å (chains), the Ni···O repulsive electrostatic energy increases approximately 300%. Moreover, the Ni···O atomic charge overlap (bond order) is 100 times smaller than in the case of the N–H···O bonding. In addition, if organometallic coordination bonding was assumed to dominate the interactions in the system, one would also expect a more symmetric arrangement with a rectangular Ni mesh [36] in contrast to what is observed experimentally. Therefore, we conclude that the cohesion in the isolated Ni–PTCDI chains is dominated by intermolecular H-bonding and they are further stabilised by attractive molecule–Au interactions (primarily by vdW forces). We speculate that the formation of isolated Ni–PTCDI rows arises from repulsive electrostatic forces between the $NiAu_3$ dipoles at the perimeter of the rows, although possible effects from electronic screening or other electrostatic contributions were not quantified from our calculations.

Figure 3(f) shows a "T-shaped" junction observed where two PTCDI/Ni chains meet on the terraces. The formation of such "T-junctions" suggests that it is possible for the PTCDI/Ni structure to develop from the observed 1-D chains into 2-D networks.

When the coverage is further increased, islands of an extended porous network can be formed as depicted in Fig. 4(a). These data were obtained after simultaneous co-deposition of PTCDI (~0.3–0.4 ML) and Ni (~0.04 ML) onto a Au(111) substrate kept at room temperature, followed by post-deposition annealing at 400 K for 10 min and cooling to 110 K. Extended and well-ordered 2-D networks can only be obtained by simultaneous deposition. With sequential deposition, pure PTCDI islands and Ni clusters tend to form. This observation is ascribed to kinetic difficulties with dissolving the phase-separated structures during annealing in the high-coverage situation

Figure 4(b) shows an STM image of the interior of an island, revealing its 2-D matrix structure at higher resolution. The STM image shows a number of identical, elongated entities which, from their dimensions and appearance, are attributed to PTCDI molecules, in accordance with the structures discussed above. These PTCDI molecules participate in the 2-D matrix structure in two different organisational motifs: Some (marked "A" in Fig. 4(b)) form rails by head-to-tail stacking with a periodicity of 1.4 ± 0.1 nm (identical to that observed in the 1-D chains) while others form crossties connecting to the rails similarly to the "T-junction" shown in Fig. 3(e). The crosstie PTCDI molecules can assume two different orientations (marked "B" and "C" in Fig. 4(b)).

Carefully scaled models of PTCDI molecules have been superimposed on the STM image in Fig. 4(b), suggesting that the "A" type molecules align head-to-tail with the same relative orientation and periodicity as in the rows formed within the PTCDI islands and the 1-D Ni–PTCDI chains, allowing for intermolecular double N–H···O H-bonding. The crude structural model furthermore suggests that if PTCDI molecules were the only entities forming the observed 2-D matrix structure, the crosstie molecules marked "B" and "C" would be in rather different chemical environments: From the zoom-in of the structure depicted in Fig. 4(c), it is clear that while "C-type" molecules may plausibly couple to nearest neighbouring "A-type" molecules by single N–H···O hydrogen bonds (although the bonding angle is not optimal), there is no possibility for "B-type" molecules to form strong hydrogen bonds with "A". However, based on statistical analysis of STM images we find that of 300 crosstie molecules, the proportion of molecules in configuration "B" and "C" is essentially equal (148 for "B" versus 152 for "C"), showing that they must be bound within the structure with similar energies. This similarity indicates that even if hydrogen bonds between "A" and "C" could exist, it is not the primary energetic

contribution to the formation of the 2-D matrix structure. Moreover, since the 2-D matrix structure was only observed when PTCDI and Ni were co-deposited, we must consider the role of Ni atoms in forming the structure. We therefore propose that the rail-crosstie junctions involve a Ni–PTCDI interaction motif, as would also be anticipated if the matrix structure is attributed to a 2-D extension of the 1-D Ni–PTCDI chains as suggested by the observation of T-junctions described above.

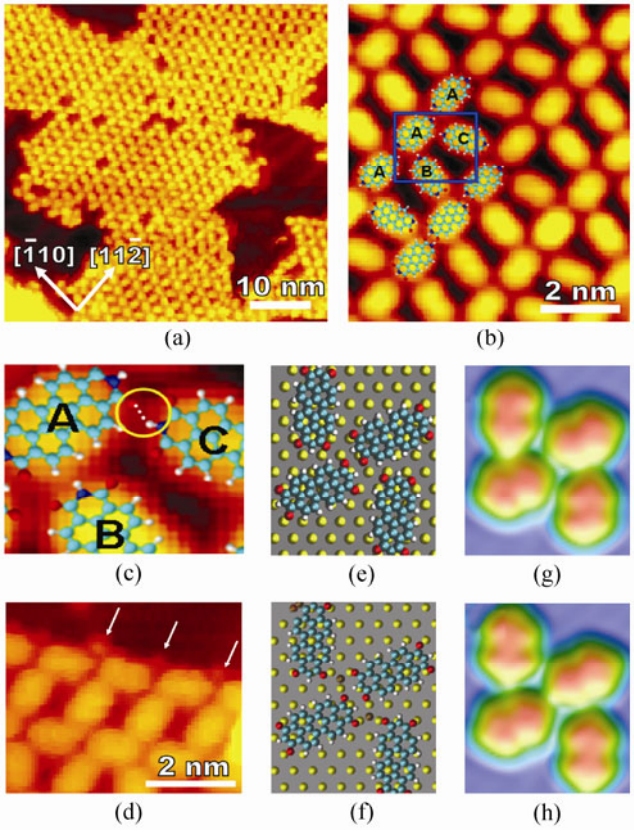

Figure 4 (a) STM image showing domains of the 2-D PTCDI/Ni matrix structure Au(111) (I_t = 0.50 nA, V_t = 1.92 V). (b) High-resolution STM image of the matrix superimposed by carefully scaled models of PTCDI molecules. Three types of molecular motifs are indicated: "A" type molecule form the rails of the structure while "B" and "C" type molecules act as crossties in different orientations (I_t = 0.50 nA, V_t = 1.75 V). (c) A zoom-in of panel b, showing that it is possible to form hydrogen bond between "A" and "C", not between "A" and "B". (d) STM image showing Ni atoms at the edge of the matrix structure as indicated by white arrows (I_t = 0.35 nA, V_t = 1.54 V). (e) and (f) Optimized model of the junctions in the 2D Ni–PTCDI matrix calculated by the MM4 force field after full relaxation. (g) and (h) Calculated STM images for the shown 2-D junctions of PTCDI without and with Ni atoms, respectively

In the STM images of the Ni–PTCDI 2-D matrix, there is however no visible contrast in the internal rail-crosstie junctions which can be attributed to the Ni atoms. To establish whether an STM signature of Ni atoms in the junctions of the matrix is to be expected, we modelled the two situations illustrated in Figs. 4(e) and 4(f) with and without Ni atoms in the junction, respectively. The corresponding calculated STM images for these structures (Figs. 4(g) and 4(h)) reveal that even when Ni atoms are present in the matrix, the STM images do not show contrast from Ni atoms, consistent with the experimental results. The missing contrast results because repulsive electrostatic Ni···O interaction destabilizes the Ni valence atomic orbitals to shift their corresponding energy levels higher than the energy range probed at the bias voltage applied during the STM imaging. The magnitude of the energy-shift is inversely proportional to the square of Ni···O interatomic separation and a larger Ni···O distance, and therefore a weaker Ni–O coupling, leads to better visible Ni atoms. Consistently, features corresponding to Ni atoms are clearly observed at the edges of the matrix structure, where the structure is expected to be comparable to that of the 1-D Ni–PTCDI chains (see Fig. 4(d), indicated by white arrows) while an STM signature of the Ni atoms in the internal part of the structure, where the Ni atom is surrounded by three close-lying O atoms, is not observed. This explanation is also consistent with the observation of a Ni atom signature in the experimental and calculated STM images of the 1-D clusters (Fig. 2) since here the Ni···O distance is considerably larger than in the nodes of the 2-D matrix. Several previous studies have also been reported where metal atoms in a network formed by metal–organic interaction did not show any contrast in STM images [12, 13, 28, 35, 37, 38].

In summary the 2-D Ni–PTCDI matrix structure involves a scaffold of aligned Ni atoms and PTCDI molecules, similarly to the 1-D structure, where the distance between rows is large enough to be occupied by PTCDI molecules with two orientations. The structure in the rails is similar to that observed in the islands of pure PTCDI and in the 1-D chains, and is ascribed to H-bonding. The detailed binding mechanism for the crosstie molecules in the junctions has not been established due to a prohibitively large

size of the system required for quantitative calculations. However, the MM4 relaxed structure in Fig. 4(f) indicates that the shortest Ni···O interatomic separation in the matrix structure is 3.2 Å which is too large to induce a strong coordination bonding (recall that the molecules adsorb in plane positioned ~3.8 Å from the gold surface plane, whereas the Ni atoms are adsorbed at a height of 1.8 Å, causing the Ni–O vector to be longer than the in-plane projection visible in the 2D model of Fig. 4(f) and in the STM images).

The Ni adatoms in the clusters and chains were found from the PM6 calculations to carry a partial negative charge. That the Ni adatom is negatively charged on the Au surface might be considered counterintuitive in terms of the Pauling electronegativity scale (where the most electronegative atom carries the negative partial charge) since the isotropic Ni electronegativity is 1.91 compared to 2.53 for Au. However, a naive electronegativity argument does not apply generally for metallic adsorbates because the anisotropy experienced by surface atoms induces a modification in the relative scale of electronegativity factors [71]. This is a consequence of the environmental change in the atomic coordination number and the hybridization state of the surface atoms and is also true for a single adatom as considered here.

Control calculations were performed by the PM6 method to compare to the calculations for PTCDI surrounded by four Ni adatoms, i.e., for a system of similar geometry but now with the PTCDI molecule removed. In this case one finds a partial charge distribution for the tetrahedral ($NiAu_3$) structures where the Ni atom has a mean charge of –0.82|*e*| and the nearest Au neighbours +0.26|*e*|. This may be compared to the value of –0.62|*e*| to –0.65|*e*| for the charge on the Ni adatoms when the PTCDI molecule is present, showing that the interaction with the PTCDI molecules induces only a minor change in the charge state of the Ni adatoms. By taking into account the stoichiometry of the ($NiAu_3$), one can notice that the negative charge on Ni is approximately three times the positive charge excess on each Au atom of the ($NiAu_3$) tetrahedral structure. Interestingly, the charge difference between the Ni and Au atoms is almost equal to 1 [i.e., –0.82 – (+0.26)]. This is physically reasonable, since it is consistent with the 18-electron rule ($s^2d^{10}p^6$) for transition metal complexes [72, 73]. To see this, consider the $NiAu_3$ structure as a "complex" according to this rule and note that in an equivalent $AuAu_3$ complex (where the Ni adatom is replaced by Au) the Au adatom would be uncharged (our control calculation finds a small charge of +0.06|*e*|) and the rule must be assumed to be fulfilled. Given the Ni (d^8s^2) ground state and the Au($d^{10}s^1$) valence electronic configuration, the eighteen electron rule is satisfied if the Ni and Au atoms remedy deficiencies of 8 and 7 electrons in their coordination spheres, respectively. Thus, an extra valence electron charge should ideally be on the Ni atom in the $NiAu_3$ cluster to make it equivalent to the $AuAu_3$ case, in qualitative agreement with our calculations.

The identification of a metalloorganic surface structure based on electrostatic interaction to metal adatoms carrying a partial negative charge is different from the situation with cationic metal centers generally assumed or found in the case of metal–organic coordination complexes on surfaces [12–38]. A surface coordination network involving negatively charged metal centers was reported [39] for the case of Cu/Cu(111) where it was shown by HF/3-21G* calculations that a Cu adatom surrounded by three 9,10-anthracenedicarbonitrile molecules exhibits an excess of negative partial charge to remedy electron donation from the substrate to the ligands. In this case, the short adatom–molecule distance (1.99 Å) results in a coordination bond. The charge transfer implies that the valence of the complexated Cu adatom is less by one electron than the Cu surface atoms. Notice that this situation is isoelectronic to the present system in which the valence of Ni (d^8s^2) uncomplexed adatom is also less by one electron than the surface Au($d^{10}s^1$) but in our case there is no coordination interaction to surrounding ligands.

The results reported here for PTCDI and Ni on Au(111) should be compared to those of a recent STM study by Jensen and Baddeley for the same system [36]. There, short (< 10 nm) chain-like segments attributed to PTCDI/Ni were found to link large Ni islands formed at the elbow sites of Au substrate. Ni atoms attached to these 1-D chains were, however, not systematically resolved, possibly due to limited resolution of the room temperature STM images. Small islands

with a structure consistent with the 2-D PTCDI/Ni matrix structure discussed here were also observed. In contrast to the present work, both structures were ascribed to metal–organic coordination bonding, and it was speculated that dehydrogenation of the N–H moieties during PTCDI evaporation allows N···Ni···N interaction. However, this proposed bonding scheme results in a different structure from our 1-D experimental and theoretical results. In particular, PTCDI molecules would assume a periodicity larger than that for the rows of the pure PTCDI structure and the Ni atoms should be positioned symmetrically around the chain, in contrast to what is observed here. The model proposed for the 2-D structure also has cross-tie molecules only in a single orientation, orthogonally to the rails, in contrast to what is observed here. We finally note that a 2-D extended structure with some similarities to the one discussed here was observed for the related system PTCDA–Fe [12].

4. Conclusions

In summary, we have investigated the self-assembly of PTCDI molecules and Ni adatoms on the herringbone reconstructed Au(111) surface using a combination of STM measurements and theoretical calculations. We demonstrate that it is possible to obtain three distinct types of nanostructures with increasing Ni–PTCDI coverage: (i) 0-D clusters involving three PTCDI molecules surrounding a central Ni atom, (ii) 1-D chains formed from rows of PTCDI molecules surrounded by peripheral Ni atoms, and (iii) a 2-D matrix structure attributed to a joining of the 1-D Ni–PTCDI rows by interlinking PTCDI molecules. The Ni atoms are directly observed by high resolution STM in the 0-D and 1-D structures, consistent with STM image calculations for optimized structural models. Ni atoms are believed to be present in the nodes of the 2-D matrix structure, but do not provide contrast in the STM images due electronic coupling between Ni and the carboxyl moieties of the PTCDI molecules, as confirmed by STM image calculations. The subtle interplay among non-covalent interactions responsible for formation of the observed structures has been revealed by calculations of partial charges, bond orders and binding energies in the structures. The 0-D clusters are joined primarily by vdW forces and weak H-bonds, while the Ni atoms provide nucleation sites on the surface. In the 1-D chains the PTCDI molecules are joined by double N–H···O hydrogen bonds, similarly to the situation in islands formed from PTCDI alone, and this motif is also found in the rails of the 2-D matrix structure. For the two situations where the role of the Ni was analysed in detail (0-D clusters and 1-D chains), the Ni adatoms were found to have a partial negative charge and they contributed to the cohesion in the metal–organic structures solely through electrostatic interactions while the bond order for Ni–O orbital overlap was found to be very low owing to a large molecule–adatom separation. The Ni–PTCDI system thus behaves in contrast to the typical situation for metal–organic supramolecular surface structures where cohesion arises from metal–molecule coordination or covalent bonding [13, 15–21].

Acknowledgements

We acknowledge financial support from the Marie–Curie Early Stage Training Network MONET and Initial Training Network SMALL, The Danish Council for Independent Research Natural Sciences, The Villum Foundation, and the Danish National Research Foundation for support to the Sino–Danish Center for Molecular Nanostructures on Surfaces. Part of this work was performed using High Performance Computing resources from the Calcul en Midi-Pyrénées (CALMIP) facilities (Grant No. 2011-[P0832]).

References

[1] Joachim, C.; Gimzewski, J. K.; Aviram, A. Electronics using hybrid-molecular and mono-molecular devices. *Nature* **2000**, *408*, 541–548.

[2] Davis, M. E. Ordered porous materials for emerging applications. *Nature* **2002**, *417*, 813–821.

[3] Schoonveld, W. A.; Wildeman, J.; Fichou, D.; Bobbert, P. A.; van Wees, B. J.; Klapwijk, T. M. Coulomb-blockade transport in single-crystal organic thin-film transistors. *Nature* **2000**, *404*, 977–980.

[4] Seo, J. S.; Whang, D.; Lee, H.; Jun, S. I.; Oh, J.; Jeon, Y. J.; Kim, K. A homochiral metal–organic porous material for

enantioselective separation and catalysis. *Nature* **2000**, *404*, 982–986.

[5] Bohringer, M.; Morgenstern, K.; Schneider, W. D.; Berndt, R.; Mauri, F.; De Vita, A.; Car, R. Two-dimensional self-assembly of supramolecular clusters and chains. *Phys. Rev. Lett.* **1999**, *83*, 324–327.

[6] Barth, J. V.; Weckesser, J.; Trimarchi, G.; Vladimirova, M.; De Vita, A.; Cai, C. Z.; Brune, H.; Günter, P.; Kern, K. Stereochemical effects in supramolecular self-assembly at surfaces: 1-D versus 2-D enantiomorphic ordering for PVBA and PEBA on Ag(111). *J. Am. Chem. Soc.* **2002**, *124*, 7991–8000.

[7] Cañas-Ventura, M. E.; Xiao, W.; Wasserfallen, D.; Müllen, K.; Brune, H.; Barth, J. V.; Fasel, R. Self-assembly of periodic bicomponent wires and ribbons. *Angew. Chem. Int. Ed.* **2007**, *46*, 1814–1818.

[8] Keeling, D. L.; Oxtoby, N. S.; Wilson, C.; Humphry, M. J.; Champness, N. R.; Beton, P. H. Assembly and processing of hydrogen bond induced supramolecular nanostructures. *Nano Lett.* **2003**, *3*, 9–12.

[9] Yu, M.; Kalashnyk, N.; Xu, W.; Barattin, R.; Benjalal, Y.; Laegsgaard, E.; Stensgaard, I.; Hliwa, M.; Bouju, X.; Gourdon, A.; Joachim, C.; Besenbacher, F.; Linderoth, T. R. Supramolecular architectures on surfaces formed through hydrogen bonding optimized in three dimensions. *ACS Nano* **2010**, *4*, 4097–4109.

[10] Stepanow, S.; Lin, N.; Vidal, F.; Landa, A.; Ruben, M.; Barth, J. V.; Kern, K. Programming supramolecular assembly and chirality in two-dimensional dicarboxylate networks on a Cu(100) surface. *Nano Lett.* **2005**, *5*, 901–904.

[11] De Feyter, S.; Miura, A.; Yao, S.; Chen, Z.; Würthner, F.; Jonkheijm, P.; Schenning, A.; Meijer, E. W.; De Schryver, F. C. Two-dimensional self-assembly into multicomponent hydrogen-bonded nanostructures. *Nano Lett.* **2005**, *5*, 77–81.

[12] Álvarez, L.; Peláez, S.; Caillard, R.; Serena, P. A.; Martin-Gago, J. A.; Méndez, J. Metal–organic extended 2D structures: Fe-PTCDA on Au(111). *Nanotechnology* **2010**, *21*, 305073.

[13] Clair, S.; Pons, S.; Brune, H.; Kern, K.; Barth, J. V. Mesoscopic metallosupramolecular texturing by hierarchic assembly. *Angew. Chem. Int. Ed.* **2005**, *44*, 7294–7297.

[14] Shi, Z. L.; Lin, N. Structural and chemical control in assembly of multicomponent metal–organic coordination networks on a surface. *J. Am. Chem. Soc.* **2010**, *132*, 10756–10761.

[15] Tait, S. L.; Wang, Y.; Costantini, G.; Lin, N.; Baraldi, A.; Esch, F.; Petaccia, L.; Lizzit, S.; Kern, K. Metal–organic coordination interactions in Fe-terephthalic acid networks on Cu(100). *J. Am. Chem. Soc.* **2008**, *130*, 2108–2113.

[16] Dmitriev, A.; Spillmann, H.; Lin, N.; Barth, J. V.; Kern, K. Modular assembly of two-dimensional metal–organic coordination networks at a metal surface. *Angew. Chem. Int. Ed.* **2003**, *42*, 2670–2673.

[17] Méndez, J.; Caillard, R.; Otero, G.; Nicoara, N.; Martín-Gago, J. A. Nanostructured organic material: From molecular chains to organic nanodots. *Adv. Mater.* **2006**, *18*, 2048–2052.

[18] Makoudi, Y.; Arab, M.; Palmino, F.; Duverger, E.; Ramseyer, C.; Picaud, F.; Chérioux, F. A stable room-temperature molecular assembly of zwitterionic organic dipoles guided by a Si(111)-7×7 template effect. *Angew. Chem. Int. Ed.* **2007**, *46*, 9287–9290.

[19] Heim, D.; Écija, D.; Seufert, K.; Auwärter, W.; Aurisicchio, C.; Fabbro, C.; Bonifazi, D.; Barth, J. V. Self-assembly of flexible one-dimensional coordination polymers on metal surfaces. *J. Am. Chem. Soc.* **2010**, *132*, 6783–6790.

[20] Liljeroth, P.; Swart, I.; Paavilainen, S.; Repp, J.; Meyer, G. Single-molecule synthesis and characterization of metal–ligand complexes by low-temperature STM. *Nano Lett.* **2010**, *10*, 2475–2479.

[21] Haq, S.; Hanke, F.; Dyer, M. S.; Persson, M.; Iavicoli, P.; Amabilino, D. B.; Raval, R. Clean coupling of unfunctionalized porphyrins at surfaces to give highly oriented organometallic oligomers. *J. Am. Chem. Soc.* **2011**, *133*, 12031–12039.

[22] Guillermet, O.; Niemi, E.; Nagarajan, S.; Bouju, X.; Martrou, D.; Gourdon, A.; Gauthier, S. Self-assembly of fivefold-symmetric molecules on a threefold-symmetric surface. *Angew. Chem. Int. Ed.* **2009**, *48*, 1970–1973.

[23] Villagomez, C. J.; Guillermet, O.; Goudeau, S.; Ample, F.; Xu, H.; Coudret, C.; Bouju, X.; Zambelli, T.; Gauthier, S. Self-assembly of enantiopure domains: The case of indigo on Cu(111). *J. Chem. Phys.* **2010**, *132*, 074705.

[24] Tseng, T. C.; Abdurakhmanova, N.; Stepanow, S.; Kern, K. Hierarchical assembly and reticulation of two-dimensional Mn– and Ni–TCNQ$_x$ (x = 1, 2, 4) coordination structures on a metal surface. *J. Phys. Chem. C* **2011**, *115*, 10211–10217.

[25] Krenner, W.; Klappenberger, F.; Kühne, D.; Diller, K.; Qu, Z. R.; Ruben, M.; Barth, J. V. Positioning of single Co atoms steered by a self-assembled organic molecular template. *J. Phys. Chem. Lett.* **2011**, *2*, 1639–1645.

[26] Cañas-Ventura, M. E.; Aït-Mansour, K.; Ruffieux, P.; Rieger, R.; Müllen, K.; Brune, H.; Fasel, R. Complex interplay and hierarchy of interactions in two-dimensional supramolecular assemblies. *ACS Nano* **2011**, *5*, 457–469.

[27] Seitsonen, A. P.; Lingenfelder, M.; Spillmann, H.; Dmitriev, A.; Stepanow, S.; Lin, N.; Kern, K.; Barth, J. V. Density functional theory analysis of carboxylate-bridged diiron units in two-dimensional metal–organic grids. *J. Am. Chem. Soc.* **2006**, *128*, 5634–5635.

[28] Schlickum, U.; Decker, R.; Klappenberger, F.; Zoppellaro, G.; Klyatskaya, S.; Ruben, M.; Silanes, I.; Arnau, A.; Kern, K.; Brune, H.; Barth, J. V. Metal–organic honeycomb nanomeshes with tunable cavity size. *Nano Lett.* **2007**, *7*, 3813–3817.

[29] Barth, J. V. Fresh perspectives for surface coordination chemistry. *Surf. Sci.* **2009**, *603*, 1533–1541.

[30] Björk, J.; Matena, M.; Dyer, M. S.; Enache, M.; Lobo-Checa, J.; Gade, L. H.; Jung, T. A.; Stöhr, M.; Persson, M. STM fingerprint of molecule-adatom interactions in a self-assembled metal–organic surface coordination network on Cu(111). *Phys. Chem. Chem. Phys.* **2010**, *12*, 8815–8821.

[31] Walch, H.; Dienstmaier, J.; Eder, G.; Gutzler, R.; Schlögl, S.; Sirtl, T.; Das, K.; Schmittel, M.; Lackinger, M. Extended two-dimensional metal–organic frameworks based on thiolate–copper coordination bonds. *J. Am. Chem. Soc.* **2011**, *133*, 7909–7915.

[32] Henningsen, N.; Rurali, R.; Limbach, C.; Drost, R.; Pascual, J. I.; Franke, K. J. Site-dependent coordination bonding in self-assembled metal–organic networks. *J. Phys. Chem. Lett.* **2011**, *2*, 55–61.

[33] Li, Y.; Xiao, J.; Shubina, T. E.; Chen, M.; Shi, Z.; Schmid, M.; Steinröck, H. P.; Gottfried, J. M.; Lin, N. Coordination and metalation bifunctionality of Cu with 5,10,15,20-tetra (4-pyridyl) porphyrin: Toward a mixed-valence two-dimensional coordination network. *J. Am. Chem. Soc.* **2012**, *134*, 6401–6408.

[34] Kley, C. S.; Čechal, J.; Kumagai, T.; Schramm, F.; Ruben, M.; Stepanow, S.; Kern, K. Highly adaptable two-dimensional metal–organic coordination networks on metal surfaces. *J. Am. Chem. Soc.* **2012**, *134*, 6072–6075.

[35] Trant, A. G.; Jones, T. E.; Baddeley, C. J. Thermal treatment of glutamic acid-modified nickel nanoclusters on Au{111} leads to the formation of one-dimensional metal–organic coordination networks. *J. Phys. Chem. C* **2007**, *111*, 10534–10540.

[36] Jensen, S.; Baddeley, C. J. Formation of PTCDI-based metal organic structures on a Au(111) surface modified by 2-D Ni clusters. *J. Phys. Chem. C* **2008**, *112*, 15439–15448.

[37] Stepanow, S.; Lin, N.; Payer, D.; Schlickum, U.; Klappenberger, F.; Zoppellaro, G.; Ruben, M.; Brune, H.; Barth, J. V.; Kern, K. Surface-assisted assembly of 2D metal–organic networks that exhibit unusual threefold coordination symmetry. *Angew. Chem. Int. Ed.* **2007**, *46*, 710–713.

[38] Clair, S.; Pons, S.; Fabris, S.; Baroni, S.; Brune, H.; Kern, K.; Barth, J. V. Monitoring two-dimensional coordination reactions: Directed assembly of Co-terephthalate nanosystems on Au(111). *J. Phys. Chem. B* **2006**, *110*, 5627–5632.

[39] Pawin, G.; Wong, K. L.; Kim, D.; Sun, D.; Bartels, L.; Hong, S.; Rahman, T. S.; Carp, R.; Marsella, M. A surface coordination network based on substrate-derived metal adatoms with local charge excess. *Angew. Chem. Int. Ed.* **2008**, *47*, 8442–8445.

[40] Balakrishnan, K.; Datar, A.; Oitker, R.; Chen, H.; Zuo, J. M.; Zang, L. Nanobelt self-assembly from an organic n-type semiconductor: Propoxyethyl-PTCDI. *J. Am. Chem. Soc.* **2005**, *127*, 10496–10497.

[41] Friend, R. H.; Gymer, R. W.; Holmes, A. B.; Burroughes, J. H.; Marks, R. N.; Taliani, C.; Bradley, D. D. C.; Dos Santos, D. A.; Brédas, J. L.; Lögdlund, M.; Salaneck, W. R. Electroluminescence in conjugated polymers. *Nature* **1999**, *397*, 121–128.

[42] Ludwig, C.; Gompf, B.; Petersen, J.; Strohmaier, R.; Eisenmenger, W. STM investigations of PTCDA and PTCDI on graphite and MoS_2—a systematic study of epitaxy and STM image-contrast. *Z. Phys. B* **1994**, *93*, 365–373.

[43] Guillermet, O.; Glachant, A.; Hoarau, J. Y.; Mossoyan, J. C.; Mossoyan, M. Perylene tetracarboxylic diimide ultrathin film deposition on Pt(100): A LEED, AES, REELS and STM study. *Surf. Sci.* **2004**, *548*, 129–137.

[44] Swarbrick, J. C.; Ma, J.; Theobald, J. A.; Oxtoby, N. S.; O'Shea, J. N.; Champness, N. R.; Beton, P. H. Square, hexagonal, and row phases of PTCDA and PTCDI on Ag–Si(111) $\sqrt{3} \times \sqrt{3} R30°$. *J. Phys. Chem. B* **2005**, *109*, 12167–12174.

[45] Mura, M.; Silly, F.; Briggs, G. A. D.; Castell, M. R.; Kantorovich, L. N. H-bonding supramolecular assemblies of PTCDI molecules on the Au(111) surface. *J. Phys. Chem. C* **2009**, *113*, 21840–21848.

[46] Topple, J. M.; Burke, S. A.; Fostner, S.; Grutter, P. Thin film evolution: Dewetting dynamics of a bimodal molecular system. *Phys. Rev. B* **2009**, *79*, 205414.

[47] Ait-Mansour, K.; Treier, M.; Ruffieux, P.; Bieri, M.; Jaafar, R.; Gröning, P.; Fasel, R.; Groning, O. Template-directed molecular nanostructures on the Ag/Pt(111) dislocation network. *J. Phys. Chem. C* **2009**, *113*, 8407–8411.

[48] O'Shea, J. N.; Saywell, A.; Magnano, G.; Perdigão, L. M. A.; Satterley, C. J.; Beton, P. H.; Dhanak, V. R. Adsorption of PTCDI on Au(111): Photoemission and scanning tunnelling microscopy. *Surf. Sci.* **2009**, *603*, 3094–3098.

[49] Perdigao, L. M. A.; Perkins, E. W.; Ma, J.; Staniec, P. A.; Rogers, B. L.; Champness, N. R.; Beton, P. H. Bimolecular networks and supramolecular traps on Au(111). *J. Phys. Chem. B* **2006**, *110*, 12539–12542.

[50] Theobald, J. A.; Oxtoby, N. S.; Phillips, M. A.; Champness, N. R.; Beton, P. H. Controlling molecular deposition and layer structure with supramolecular surface assemblies. *Nature* **2003**, *424*, 1029–1031.

[51] Gardener, J. A.; Shvarova, O. Y.; Briggs, G. A. D.; Castell, M. R. Intricate hydrogen-bonded networks: Binary and ternary combinations of uracil, PTCDI, and melamine. *J. Phys. Chem. C* **2010**, *114*, 5859–5866.

[52] Laegsgaard, E.; Osterlund, L.; Thostrup, P.; Rasmussen, P. B.; Stensgaard, I.; Besenbacher, F. A high-pressure scanning tunneling microscope. *Rev. Sci. Instrum.* **2001**, *72*, 3537–3542.

[53] Schmidt, M. W.; Baldridge, K. K.; Boatz, J. A.; Elbert, S. T.; Gordon, M. S.; Jensen, J. H.; Koseki, S.; Matsunaga, N.; Nguyen, K. A.; Su, S. J.; Windus, T. L.; Dupuis, M.; Montgomery, J. A. General atomic and molecular electronic-structure system. *J. Comput. Chem.* **1993**, *14*, 1347–1363.

[54] Allinger, N. L.; Chen, K. S.; Lii, J. H. An improved force field (MM4) for saturated hydrocarbons. *J. Comput. Chem.* **1996**, *17*, 642–668.

[55] Allinger, N. L. Understanding molecular structure from molecular mechanics. *J. Comput. Aided Mol. Des.* **2011**, *25*, 295–316.

[56] Stewart, J. J. P. *MOPAC2009*; *Stewart Computational Chemistry*. Colorado Springs, CO, USA. http://openmopac.net/ (accessed 2008).

[57] Sautet, P.; Joachim, C. Electronic transmission coefficient for the single-impurity problem in the scattering-matrix approach. *Phys. Rev. B* **1988**, *38*, 12238–12247.

[58] Sautet, P.; Joachim, C. Calculation of the benzene on rhodium STM images. *Chem. Phys. Lett.* **1991**, *185*, 23–30.

[59] Bouju, X.; Joachim, C.; Girard, C.; Tang, H. Mechanics of (Xe)(N) atomic chains under STM manipulation. *Phys. Rev. B* **2001**, *63*, 085415.

[60] Yu, M.; Xu, W.; Benjalal, Y.; Barattin, R.; Laegsgaard, E.; Stensgaard, I.; Hliwa, M.; Bouju, X.; Gourdon, A.; Joachim, C.; Linderoth, T. R.; Besenbacher, F. STM manipulation of molecular moulds on metal surfaces. *Nano Res.* **2009**, *2*, 254–259.

[61] Barlow, S. M.; Raval, R. Complex organic molecules at metal surfaces: Bonding, organisation and chirality. *Surf. Sci. Rep.* **2003**, *50*, 201–341.

[62] Tautz, F. S. Structure and bonding of large aromatic molecules on noble metal surfaces: The example of PTCDA. *Prog. Surf. Sci.* **2007**, *82*, 479–520.

[63] Xu, W.; Dong, M. D.; Gersen, H.; Rauls, E.; Vázquez-Campos, S.; Crego-Calama, M.; Reinhoudt, D. N.; Stensgaard, I.; Laegsgaard, E.; Linderoth, T. R.; Besenbacher, F. Cyanuric acid and melamine on Au(111): Structure and energetics of hydrogen-bonded networks. *Small* **2007**, *3*, 854–858.

[64] Lii, J. H.; Allinger, N. L. Directional hydrogen bonding in the MM3 force field: II. *J. Comput. Chem.* **1998**, *19*, 1001–1016.

[65] Chambliss, D. D.; Wilson, R. J.; Chiang, S. Nucleation of ordered Ni island arrays on Au(111) by surface-lattice dislocations. *Phys. Rev. Lett.* **1991**, *66*, 1721–1724.

[66] Chambliss, D. D.; Wilson, R. J.; Chiang, S. Ordered nucleation of Ni and Au islands on Au(111) studied by scanning tunneling microscopy. *J. Vac. Sci. Technol. B* **1991**, *9*, 933–937.

[67] Asta, M.; Foiles, S. M. Embedded-atom-method effective-pair-interaction study of the structural and thermodynamic properties of Cu–Ni, Cu–Ag, and Au–Ni solid solutions. *Phys. Rev. B* **1996**, *53*, 2389–2404.

[68] Van Vleck, J. H. Theory of the variations in paramagnetic anisotropy among different salts of the iron group. *Phys. Rev.* **1932**, *41*, 208–215.

[69] Figgis, B. N.; Hitchman, M. A. *Ligand Field Theory and Its Applications*; Wiley-VCH: New York, 2000.

[70] Stewart, J. J. P. Optimization of parameters for semiempirical methods V: Modification of NDDO approximations and application to 70 elements. *J. Mol. Model.* **2007**, *13*, 1173–1213.

[71] Rodriguez, J. A.; Campbell, R. A.; Goodman, D. W. Electron donor–electron acceptor interactions in surface metal–metal bonds: The Cu/Re(0001) and Pd/Re(0001) systems. *J. Vac. Sci. Technol. A* **1992**, *10*, 2540–2545.

[72] Langmuir, I. Type of valence. *Science* **1921**, *54*, 59–67.

[73] Pyykkö, P. Understanding the eighteen-electron rule. *J. Organomet. Chem.* **2006**, *691*, 4336–4340.